Earth and Planetary Science Letters 308 (2011) 151–160

Contents lists available at ScienceDirect

Earth and Planetary Science Letters

journal homepage: www.elsevier.com/locate/epsl

Tectonic regionalization without a priori information: A cluster analysis of upper mantle tomography

Vedran Lekic [a,b,*], Barbara Romanowicz [a]

[a] Berkeley Seismological Laboratory, Berkeley, CA 94720, USA
[b] Geological Sciences, Brown University, Providence, RI 02912, USA

ARTICLE INFO

Article history:
Received 13 December 2010
Received in revised form 25 May 2011
Accepted 27 May 2011
Available online 21 June 2011

Editor: P. Shearer

Keywords:
global tomography
continental lithosphere
hotspots
cluster analysis
waveform modeling

ABSTRACT

Global mantle tomography can be improved through better use of data and application of more accurate wave propagation methods. However, few techniques have been developed for objective validation and exploration of the resulting tomographic models. We show that cluster analysis can be used to validate and explore the salient features across such models. We present a cluster analysis of a global upper mantle radially anisotropic model SEMum developed using full waveform tomography and the Spectral Element Method. Applied to SEMum down to 350 km depth, the cluster analysis reveals that absolute shear wave velocity (Vs) depth profiles naturally group into families that correspond with known surface tectonics. This allows us to construct a global tectonic regionalization based solely on tomography, without the help of any a priori information. We find that the profiles of stable platforms and shields consistently exhibit a mid-lithospheric low velocity zone (LVZ) between 80 and 130 km depth, while the asthenosphere is found at depths greater than 250 km in both regions. This global intra-continental-lithosphere low velocity zone agrees with recent receiver function studies and regional tomographic studies. Furthermore, we identify an anomalous oceanic region characterized by slow shear wave speeds at depths below 150 km. Hotspots are found preferentially in the vicinity of this anomalous region. In the Pacific Ocean, where plate velocities are largest, these regions have elongated shapes that align with absolute plate motion, suggesting a relationship between the location of hotspots and small-scale convection in the oceanic upper mantle.

1. Introduction

Until now, global mantle tomography has relied on approximate seismic wave computational tools that provide robust images of long wavelength mantle structure. Resolving smaller structure, especially in low velocity regions, remains a challenge for two reasons. First, the uneven sampling of the mantle by commonly analyzed phases — those well separated on the seismogram — must be overcome. This can be done by full-waveform modeling, which can extract the complete information contained in seismic records. Second, more accurate 3D wave propagation tools need to be employed. This is because ray approximations break down as the wavelength of the sought-after structure approaches that of the input waveforms (Spetzler et al., 2002). Furthermore, unmodeled effects of crustal structure can obscure the mantle signal (Bozdağ and Trampert, 2008; Lekic et al., 2010). Fortunately, the advent of new, fully numerical codes like the Spectral Element Method (SEM) enables accurate calculation of wave propagation through highly heterogeneous structures, including the crust (Komatitsch and Vilotte, 1998).

We developed SEMum (Lekic and Romanowicz, 2011), a high resolution model of upper mantle structure, using a fully numerical wave propagation code C-SEM (Capdeville et al., 2003) that is capable of accurately representing both the scattering and (de)focusing of seismic waves by elastic heterogeneity, and, with some approximation, the effects of the oceans, topography/bathymetry, ellipticity, gravity, rotation and anelasticity (Komatitsch and Tromp, 2002). C-SEM allows for efficient computations by restricting the SEM numerical computation to a region of the globe (here the mantle), through coupling with a fast 1D mode calculation (here in the core). We optimized data utilization through the use of full-waveform modeling of long period waveforms, with a cut-off period of 60 s to keep computational costs realistic. We minimized crustal contamination by including constraints from both long period waveforms and higher-frequency group velocity dispersion maps. We also keep computational costs reasonable by computing finite-frequency Frechet kernels — relating structure perturbations to waveform perturbations — using approximate, non-linear 2D finite-frequency kernels based on normal mode perturbation theory (Li and Romanowicz, 1995), which brings out the ray character of overtones. While the approximate partial derivatives may slow down convergence, our use of C-SEM ensures that the cost function — and therefore the tomographic model itself — is calculated more accurately than has previously been possible. Data used, parameterization, forward

* Corresponding author at: Berkeley Seismological Laboratory, Berkeley, CA 94720, USA.
E-mail address: lekic@seismo.berkeley.edu (V. Lekic).

0012-821X/$ – see front matter © 2011 Elsevier B.V. All rights reserved.
doi:10.1016/j.epsl.2011.05.050

modeling and inversion scheme, and treatment of crustal structure are described in detail in Lekic and Romanowicz (2011), and the model is available at http://www.seismo.berkeley.edu/~ekic/SEMum.html. Here, we focus on the application of a cluster analysis to the upper 350 km of SEMum.

Despite the proliferation of global tomographic velocity models (Romanowicz, 2003), few tools exist for quantitative exploration, comparison, and validation of these models. Cluster analysis allows classification of a dataset into several groups (clusters), whose members tend to be similar in some fashion (see, e.g. Romesburg, 1984). The classification is objective in the sense that the groups emerge spontaneously, and are not chosen by an operator; indeed, the only way to influence the results of the clustering is by defining the metric that quantifies similarity between individual and groups of data points. Cluster analysis has been applied across physical and social sciences. In geophysics, it has been used with success to classify structures based on a variety of data (e.g. Dumay and Fournier, 1988; Tronicke et al., 2004); in global seismology, its use has been confined to time series analysis (Houser et al., 2008). Here, we discuss the results of cluster analysis applied to the SEMum tomographic model itself, represented by isotropic shear wave speed V_S profiles in the uppermost 350 km. The goals of the analysis are twofold: 1. to identify geographical regions that share common shear velocity structure; 2. to objectively define and investigate representative velocity profiles characteristic of each of these geographic regions.

By identifying geographic regions that share similar V_S profiles in an objective and self-consistent fashion, cluster analysis makes it possible to develop a seismic regionalization without the use of any a priori information. A number of regionalization schemes have been developed previously (Gudmundsson and Sambridge, 1998; Jordan, 1981; Nataf and Ricard, 1996), which divide the Earth's surface into provinces based on geological observations. Because seismic structure correlates with tectonic setting (Romanowicz, 1991), these regionalizations could be used to predict seismic structure. A motivation for doing this was to compensate for the small amplitudes of velocity anomalies in older tomographic models. However, such regionalizations involved assumptions about extrapolations to regions with poor data coverage. Also, as they were dominated by surface observations, the regionalization-based models poorly fit observed long period surface waves, which sample deeper structures (Ekstrom et al., 1997).

We show that, now, global upper mantle V_S structure has been mapped with sufficient accuracy and uniformity to define a tectonic regionalization based solely on tomography. Indeed, a cluster-analysis based regionalization of SEMum shows compelling agreement with regionalizations based on our surface-based inferences on tectonics. Comparison of regionalizations obtained via cluster analysis of different tomographic models offers a new means of exploring tomographic models. Furthermore, inconsistencies and incongruities between these seismic regionalizations and geologic/tectonic inferences can be used as a novel means of validating seismic models and shedding light on regions where the geological structure may not be well indicative of upper mantle structure. We will demonstrate how such arguments can be brought to bear on SEMum and two other recent tomographic models and argue that SEMum more successfully recovers the well known main tectonic provinces. Finally, because the centroid of each cluster specifies a characteristic Vs profile for its corresponding geographic region, cluster analysis provides us with V_S profiles that bring out the salient characteristics of each region. Here, we focus on characteristic V_S profiles to investigate the structure of the continental lithosphere and regions affected by hotspot volcanism.

2. Cluster analysis of global tomography

We apply a k-means clustering scheme to the profiles of absolute shear wave speed (V_S) and radial anisotropy parameter ($\xi = \frac{V_{SH}^2}{V_{SV}^2}$) in SEMum beneath a regular Gaussian grid of points (2° spacing) on the Earth in the 30–350 km depth range (sampled every 10 km). This grid is finer than the nominal model resolution, which is found from resolution tests to be 1500 km laterally and ~50 km in depth (Lekic and Romanowicz, 2011), in order to avoid spatial aliasing. *k-means* is a process well-suited to very large datasets, in which a set of M-dimensional observations (e.g. vectors containing absolute Vs at a discrete number of depths) is partitioned into k sets ("clusters") so that the within-set variance is small. Thus, k-means cluster analysis requires choosing a pre-determined number of clusters (N) and will produce N reference M-dimensional points that define the clusters. MacQueen, 1967 states the procedure clearly and succinctly: *"the k-means procedure consists of simply starting with k groups each of which consists of a single random point, and thereafter adding each new point to the group whose mean the new point is nearest. After a point is added to a group, the mean of that group is adjusted in order to take account of the new point. Thus at each stage the k-means are, in fact, the means of the groups they represent (hence the term k-means)."*

A distance measure is needed to give meaning to concepts *near* and *far*. We explore two simple distance measures: 1. squared Euclidean distance, where profiles of Vs or ξ specified at *m* discrete depths are treated as vectors in *m*-dimensional space; and, 2. correlation distance, where 1 − correlation between two Vs profile vectors defines the distance between them. While correlation is the distance metric that is most-often adopted in cluster analyses of time series, it discards information on the amplitudes of velocity variations. Squared Euclidean distance, on the other hand, depends strongly on the amplitudes of Vs variations.

The starting set of k vectors is itself the result of a clustering of a decimated set of Vs profiles, which is initialized with k randomly selected profiles. Because the k-means procedure is not guaranteed to converge to the set of clusters that minimize the intra-cluster variance, we replicate the entire procedure 5 times, and take the regionalization with smallest intra-cluster variance. Our k-means clustering results are very compatible with those found using agglomerative hierarchical clustering with complete linkage, though the clusters emerge in different order. We use the MATLAB implementation of the k-means algorithm. We also carry out hierarchical agglomerative cluster analysis, and find that complete linkage — where distance between two groups of vectors is taken to be the largest distance between their constituent members — yields very similar results to those obtained from k-means clustering. In contrast, simple or average linkage forms clusters with very different numbers of members, and appears to be strongly affected by outlier profiles whose similarity to one another results in merging otherwise dissimilar clusters.

3. Patterns of upper mantle heterogeneity

3.1. Vs structure

We start with profiles of isotropic shear wave speed and by allowing two clusters to form. The geographic extents of the clusters obtained with a squared Euclidean (left) and correlation-based (right) distance measure are shown in Fig. 1. For both distance measures, the first two clusters (Fig. 1a,i) trace out the continent/ocean dichotomy, confirming that this dichotomy is the dominant pattern of upper mantle structure (Dziewonski, 1970; Kanamori, 1970; Toksöz and Anderson, 1966). One cluster covers ~60% of the earth's surface including most of the oceans as well as several Phanerozoic orogenic and magmatic zones. The other cluster covers areas undisturbed since the Phanerozoic. For the squared Euclidean distance measure, the very oldest ocean in the northwestern Pacific is grouped within the largely continental region. This is due to the fast velocities of the oldest oceanic lithosphere, to which the squared Euclidean distance measure is inherently more sensitive, and is consistent with findings of Okal (1977). Introducing a third cluster (Fig. 1b, j) separates the oceanic region into two according to age: one with a mean age of 40 Ma and

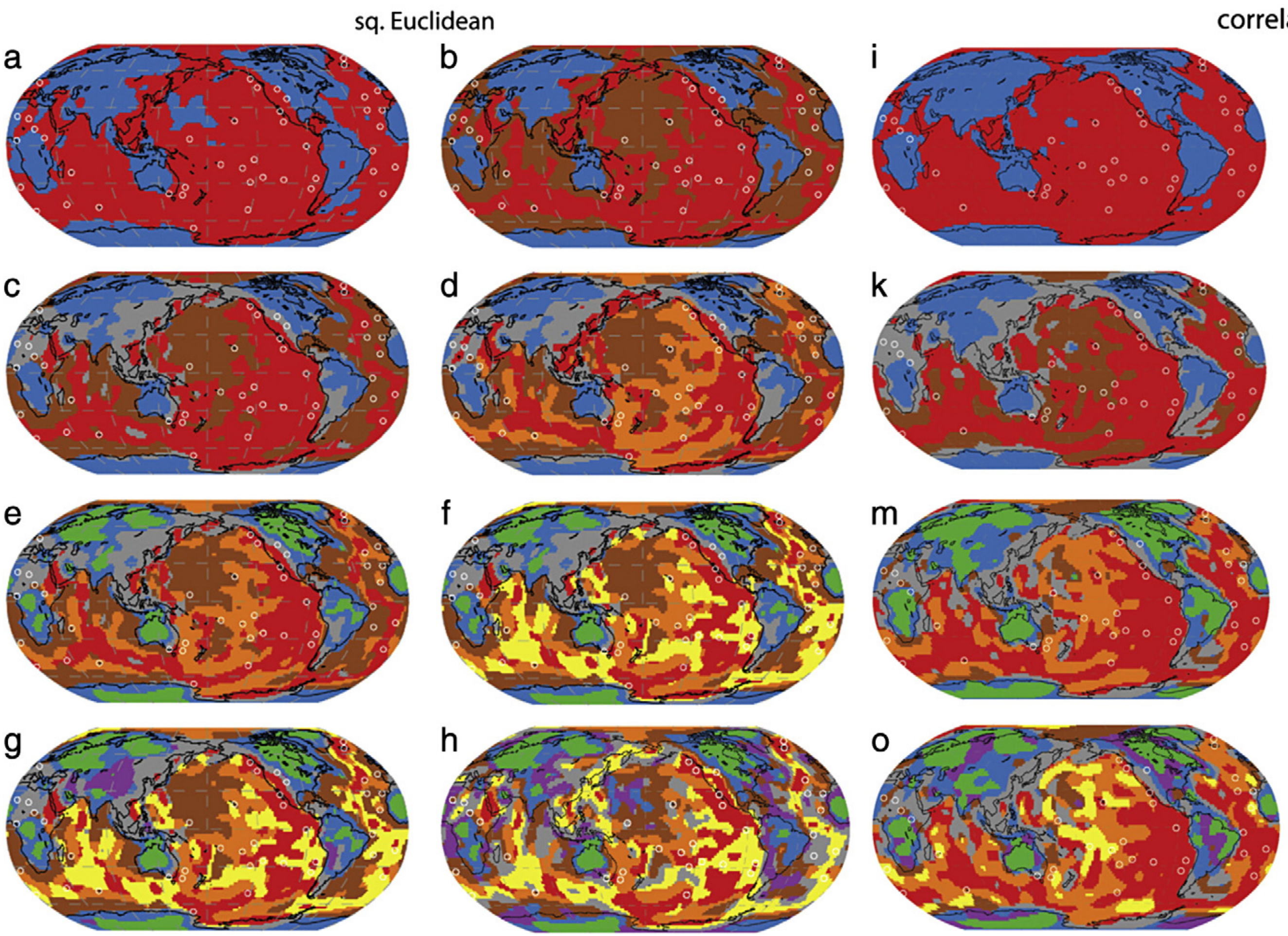

Fig. 1. Geographic extents of N clusters identified using k-means clustering of SEMum radially anisotropic upper mantle model using squared Euclidean (left) and correlation-based (right) distance measure. (a,i) N = 2; (b,j) N = 3; (c,k) N = 4; (d,l) N = 5; (e,m) N = 6; (f,n) N = 7; (g,o) N = 8. Note the appearance of continental cratons in (e). The geographic extent of clusters with squared Euclidean distance for the N = 8 case and a 60–350 depth range is plotted in panel (h). White circles denote hotspot locations from compilation of Steinberger (2000).

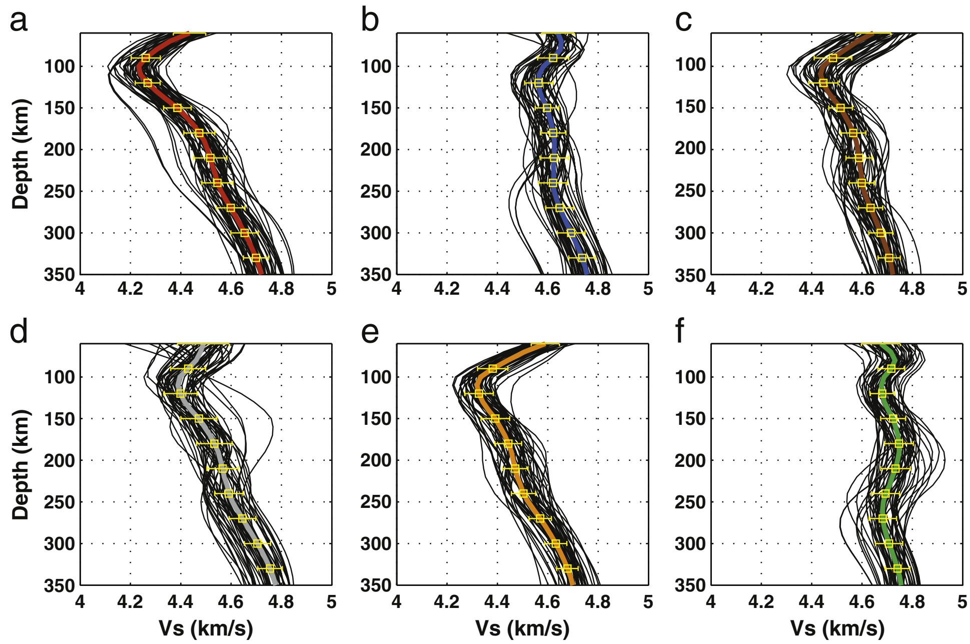

Fig. 2. Fifty randomly-chosen constituent profiles of absolute Vs in each of the clusters in the N = 6 case (Fig. 1e) are shown in black. The harmonic mean Vs for each cluster is denoted by the colored lines. Standard deviations of Vs about this mean are shown by error bars. (a) OR1; (b) CR2; (c) OR3; (d) CR3; (e) OR2; (f) CR1. The anomalously slow profiles in (a) are found beneath Iceland, the Afar, and the Galapagos, all of which are hotspots that interact with a mid-ocean ridge.

the other 92 Ma (Muller, 1997). The fourth cluster (Fig. 1c, k) traces subduction zones and continental magmatic/orogenic zones. The fifth cluster (Fig. 1d, l) separates out Mid-Ocean Ridges (MORs), back arcs, and the youngest regions around the fast-spreading East Pacific Rise (EPR), though the choice of distance measure affects the shape of this region (compare Fig. 1d and l). The sixth cluster distinguishes cratons from surrounding stable regions (Fig. 1e, m). The fact that the geographic extent of this cratonic region is similar for both distance measures indicates that this cluster is not only distinguished by the strength of the fast anomalies, but, rather, that the velocity profiles beneath cratons — regardless of which continent they are located in — have a characteristic shape. Allowing more clusters further subdivides oceanic lithosphere (Fig. 1f) and identifies unique structures within the continental regions such as Tibet and the Altiplano (Fig. 1g). Because the Tibet/Altiplano cluster appears only when the squared Euclidean distance measure is used, we conclude that the defining characteristic of this region is the very slow velocities resulting from anomalously thick crust, rather than a unique velocity profile in the mantle.

The 30–350 km depth range we use for defining the velocity profiles makes the results of the clustering depend, in part, on crustal structure. In order to determine the effect that crustal structure has on the geographical distribution of clusters, we perform a cluster analysis on profiles defined in the 60–350 km depth range using the squared Euclidean distance, so that no crustal structure is directly included in the analysis. The geographic distribution of clusters for the N = 8 case for the 60–350 km depth range is shown in Fig. 1h. The only cluster whose geographic distribution appears to be strongly affected by crustal structure is that corresponding to Tibet and the Altiplano. In addition, crustal structure appears to play a role in distinguishing the oldest oceanic lithosphere from that found beneath continents, as manifested by the presence of continental-type clusters beneath parts of the ocean basins (Fig. 1h).

We now restrict our attention to the N = 6 case for the squared Euclidean distance measure (Fig. 1e).

In order to get a better sense of the variability of velocity profiles within each cluster/region, we show fifty randomly-chosen constituent profiles of absolute Vs in each of the clusters of the N = 6 case (black lines in Fig. 2). The harmonic mean Vs for each cluster is denoted in Fig. 2 by the lines colored according to the same scheme as in Fig. 1, and the clusters are named CR1 (blue), CR2 (green), CR3 (gray), for the three continental regions, and OR1 (red), OR2 (orange), OR3 (brown), for the three oceanic regions, according to the colors used in Fig. 1d and for the remainder of this paper. The vast majority of curves posses similar shape and absolute velocities as the cluster averages. This implies that the structures evident in the average cluster V_S profiles, such as a low-velocity zone at ~100 km depth beneath stable continental settings, is representative of actual velocity profiles and is not the result of averaging curves with disparate characteristics. Nevertheless, a number of outliers can be seen, which allow anomalous regions to be identified. For example, the anomalously slow profiles in the mid-ocean ridge cluster are found beneath Iceland, the Afar, and the Galapagos hotspots, all of which are hotspots that interact with a mid-ocean ridge (Fig. 2a). Finally, Vs profiles of what will become the Tibet/Altiplano cluster in the N = 8 regionalization can be seen in the cluster corresponding to continental magmatic/orogenic zones to have low velocities at 60 km depth (i.e. thick crust) and high velocities at 150 km (Fig. 2d).

In Fig. 3abc, we show maps of geographic locations of 6 regions obtained by k-means clustering of SEMum and two other recent tomographic models, SAW24B16 (Mégnin and Romanowicz, 2000) and S362ANI (Kustowski et al., 2008). As expected, in all cases, cluster analysis distinguishes cratonic regions from magmatically/tectonically active continental settings and identifies oceanic regions that are correlated with lithospheric age. This confirms the ability of cluster analysis to identify tectonic provinces without any a priori information is not restricted to, or a peculiarity of, the SEMum model.

Despite the large-scale similarities between their clustering-based regionalizations, a number of differences distinguish SEMum from the other models and suggest that it more accurately captures upper mantle structure. First, SEMum exhibits fewer incongruities, such as the mis-identification of cratonic regions beneath the oceans apparent with SAW24B16, and the mapping of oceanic regions beneath Africa in S362ANI. Second, the cluster associated with subduction zones and

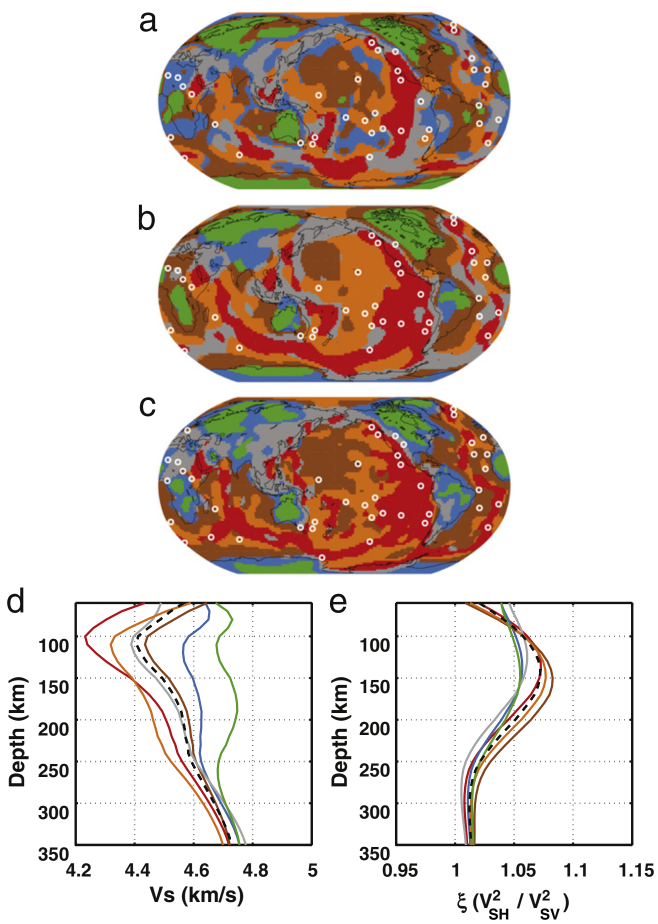

Fig. 3. Geographic extents of the 6 regions identified using k-means clustering. Application to models SAW24B16, S362ANI and SEMum, are shown in (a), (b), and (c) respectively. SEMum mean profiles of each region are shown for Voigt average Vs (d) and ξ (e).

spreading centers (red, OR1) appears to more continuously trace the world's Mid-Ocean Ridge (MOR) and back-arc system in SEMum than in either of the other models. Third, clustering on SEMum shows compelling agreement with observed shield locations (CR1, green). Specifically, the East European and the East Siberian shield are mapped in agreement with their geographical extents in 3SMAC (Nataf and Ricard, 1996) and both Greenland and all three major African cratons are successfully identified. In contrast, the South American, South African, Indian and Greenland shields are not correctly classified in SAW24B16, while clustering of S362ANI fails to identify the Greenland shield and smears the East European with the East Siberian shield and the Congo with the South African shield.

In what follows we will be discussing the results of the SEMum clustering analysis. Figs. 3d and e show the average depth profiles for Vs and ξ, respectively, for the N = 6 cluster analysis of SEMum, using the same color coding as in Fig. 3c, alongside global averages (black dashed lines). As already seen in Fig. 2, Fig. 3d shows the progressively faster velocities from mid-ocean ridges to cratons down to about 150 km and the presence of a low-velocity zone under cratons and stable continents between 100 and 140 km. These and other features of these profiles will be discussed in further detail in a later section. Fig. 3e, on the other hand, indicates that the ocean–continent dichotomy accounts for the dominant signal in radial anisotropy. Beneath continents, anisotropy ($\xi = \frac{V_{SH}^2}{V_{SV}^2}$) is present ($\xi > 1.05$) in the uppermost 150 km, and decreases rapidly below. Under oceans, anisotropy is stronger, peaking at ~ 150 km, at which depth $\xi \sim 1.08$.

The average profiles of ξ associated with clusters determined solely from the profiles of isotropic Vs demonstrate that relatively weaker anisotropy is characteristic of shield, platform and orogenic/magmatic regions, though the decay of ξ with depth is slower beneath cratons (Fig. 3e). Also, radial anisotropy becomes progressively stronger with increasing age and the depth of maximum anisotropy increases with age from 130 to 150 km.

3.2. Radial anisotropy structure

Dominant patterns of radial anisotropy structure in the upper mantle can be further explored by carrying out a cluster analysis using profiles of $\xi = \frac{V_{SH}^2}{V_{SV}^2}$ from SEMum. In Fig. 4, we show the geographic extents of clusters obtained from profiles of ξ with a squared Euclidean distance measure for the N = 2 and N = 3 cases. We confirm that, as is the case with isotropic shear wave speed variations, the ocean–continent dichotomy accounts for the dominant signal in ξ,

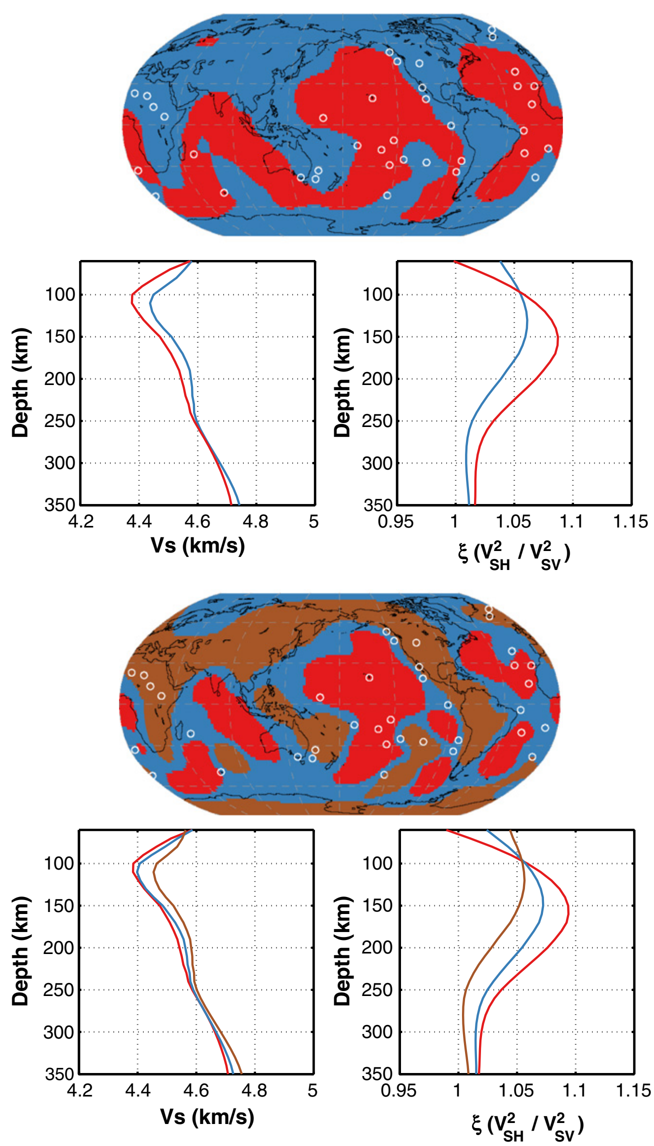

Fig. 4. Geographic extents and average Vs (left) and ξ (right) profiles of the N = 2 (top) and N = 3 (bottom) regions identified using k-means cluster analysis of ξ profiles of SEMum using a squared Euclidean distance measure. Introducing more clusters does not substantially alter the geographic extents from those apparent in the N = 3 case.

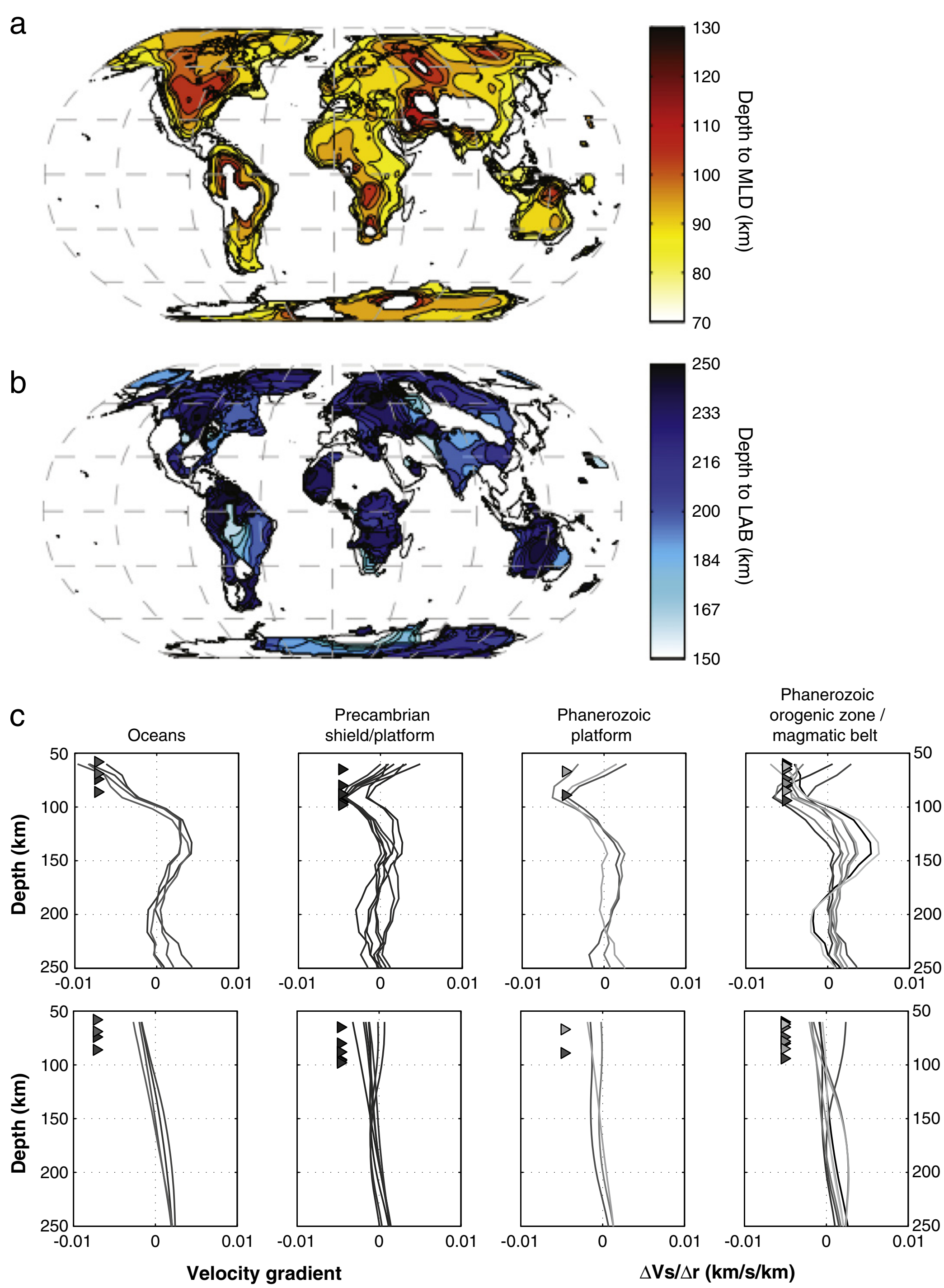

Fig. 5. Depth to the lithosphere–asthenosphere boundary (LAB) and to the top of the subcontinental mid-lithospheric low velocity zone (MLD) and comparison with RF studies. (a) The depth to the MLD is defined as the median depth in shallower of two depth ranges over which velocity gradients are consistently negative. (b) The LAB is defined as the median depth of a deeper region of negative velocity gradients that are separated from the MLD by positive velocity gradients. (c) Comparison of isotropic Vs depth-gradients in SEMum (top) and S362ANI (bottom) with the detections of LAB and MLD using receiver function (RF) analyses (triangles: Rychert and Shearer, 2009) in four tectonic settings. Velocity drops across the LAB and MLD determined from RF modeling are divided by a typical depth resolution length-scale of 50 km for comparison with tomographically-derived values. Note the excellent agreement between the depth and magnitude of Vs gradients in SEMum and RF-based detections.

and that oceanic and continental clusters are characterized by very different profiles of radial anisotropy. However, subduction zones and sections of mid-ocean ridge system are grouped with continental settings, due to their weaker anisotropy (smaller values of ξ). Allowing a third cluster to form further subdivides the largely continental cluster, indentifying a region with particularly weak anisotropy that is found beneath most continents, the Tonga–Kermadec subduction zone, and portions of the Mid-Ocean Ridges. If the seismic anisotropy results from preferential alignment of A-type fabric olivine (e.g. Karato et al. 2008), then the weakening of anisotropy may indicate vertical flow associated with downwelling in Tonga–Kermadec and localized upwelling beneath ridges. Additional clusters do not substantially alter this pattern. Using the correlation-based distance measure produces very similar clusters. In order to ascertain how incorporating

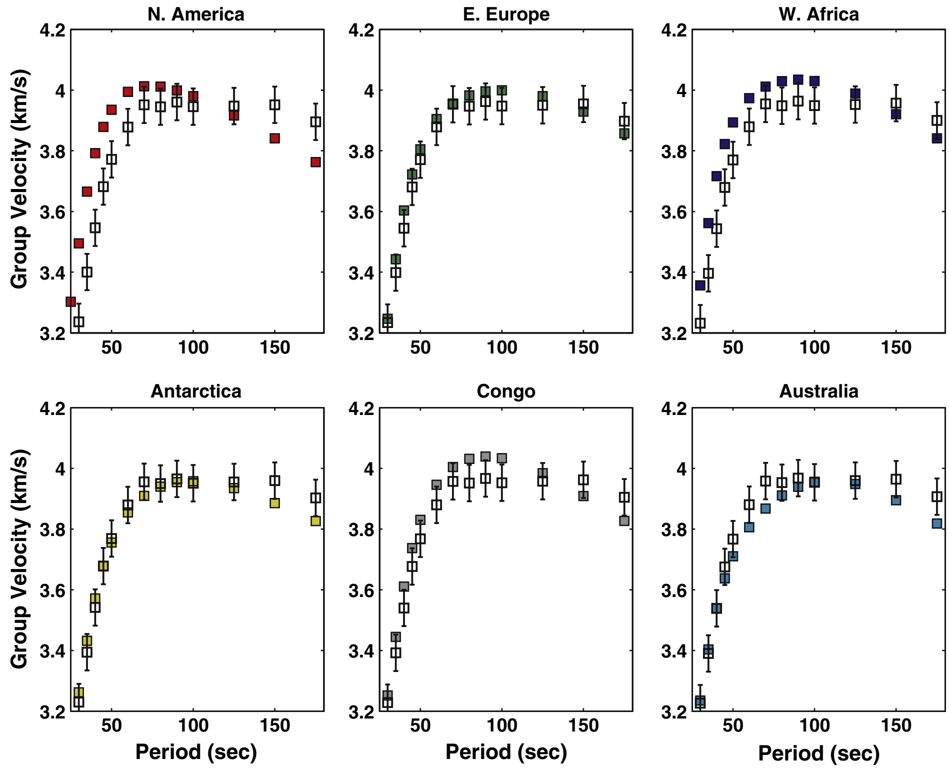

Fig. 6. Plots of Rayleigh wave group velocity dispersion curves (with nominal error bars of 0.06 km/s) beneath 6 cratons against the predictions of SEMum (colored squares).

anisotropic structure affects the geographic extents of clusters identified from isotropic Vs profiles, we carry out cluster analysis with a squared Euclidean distance measure in which both Vsv and Vsh profiles are specified beneath each point on the surface. We find that the geographic extents of clusters identified by cluster analysis of isotropic profiles are not noticeably affected.

3.3. Continental structure

A regionalization of SEMum based on 6 clusters identifies — within a single cluster (CR1) — all the world's major cratons, including smaller ones like the Arabian, Sao Fernando and Indian shields (green, Figs. 3c and 1e). CR1 is characterized by anomalously fast upper mantle seismic velocities of ~4.7 km/s down to a depth of ~250 km. CR1 is surrounded by a second region (CR2, blue) which appears to comprise other stable regions with similar, but ~100 m/s slower velocity profiles. The third cratonic region (CR3, gray) tends to be located along the margins of CR2: beneath East Asia, the Baikal Rift, Saharan hotspots, the Cameroon Volcanic Line, and western Europe. Its velocity profile is distinct from those of CR1 and CR2 showing a single velocity minimum (4.4 km/s) at ~110 km; it is the closest to the mean global Vs profile (Fig. 3d, broken lines).

Beneath continents, long-range seismic profiles show a strongly-scattering low velocity layer bounded at the top (~100 km) by the so-called $8^{\circ}_{?}$ discontinuity (Thybo and Perchuc, 1997). This finding is bolstered by detections of sharp velocity drops at ~90–110 km depth

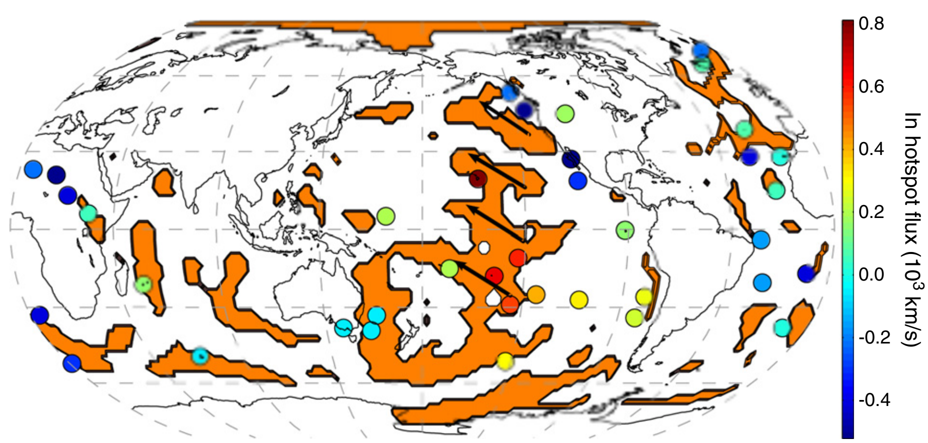

Fig. 7. The geographic extent of OR2 region compared to Pacific Plate motion (arrows, Argus and Gordon, 1991) and the location of major hotspots. (a) OR2 is shown in orange, plate motion is indicated by black arrows and hotspots are color-coded according to log of flux Steinberger (2000).

beneath stable continents using receiver functions (Abt et al., 2010; Ford et al., 2010; Rychert and Shearer, 2009), and of a mid-lithospheric discontinuity (MLD) beneath the North American craton using azimuthal anisotropy (Yuan and Romanowicz, 2010). In SEMum, both craton (CR1) and platform (CR2) clusters show two local velocity minima, a shallower one in the 100–120 km depth range, and a deeper one in the 200–300 km range. This double feature is much stronger in cratonic than in platform settings. We propose that the median depth of the strong negative velocity gradients at the top of the mid-lithospheric LVZ (ML-LVZ) define an MLD (Fig. 5a); those in the 150–250 km depth range define the LAB. Global scale maps of the MLD and LAB under stable continents inferred from the cluster analysis of SEMum are shown in Fig. 5a and b respectively. Our LAB map agrees with previous determinations based on anisotropy (Gung et al., 2003; Plomerova et al., 2002).

Long period waveforms alone may not always be able to robustly resolve an ML-LVZ (Pontevivo and Thybo, 2006), which, due to non-linearity inherent in waveform inversion, may be related to the starting 1D model. Therefore, we compare our results to an independent set of constraints. In Fig. 5c, we compare gradients of isotropic Vs from SEMum against velocity jumps inferred from receiver function (RF) analyses. Because long period tomographic models have depth resolution of ~50 km, we assume that the RF-inferred velocity jumps (Rychert and Shearer, 2009) get smeared over 50 km in depth. We find that the velocity gradients of SEMum are in excellent agreement with both the depth and magnitude of velocity drops across LAB (or MLD) determined from RF analyses. However, velocity gradients in S362ANI are substantially smaller than those required by RF observations. The agreement between SEMum and RF constraints provides a completely independent confirmation that the ML-LVZ imaged in SEMum and captured by the cluster analysis is indeed present beneath continents. Furthermore, the presence of an ML-LVZ in individual profiles further demonstrates that its presence in the clustered profiles is not an artifact of averaging disparate families of curves (also see Fig. 2). The presence of the negative velocity gradients confirms that the RFs are detecting the top of a mid-lithospheric LVZ, rather than the LAB (Romanowicz, 2009).

One may also ask how well do our data constrain such a mid-lithospheric low velocity zone? In Fig. 6, we compare observed Rayleigh wave group velocity dispersion curves (with nominal error bars of 0.06 km/s) (Ritzwoller et al., 2002) beneath 6 cratons against the predictions of SEMum (squares). We consider group velocity rather than phase velocity because the former is more sensitive to the presence/absence of a mid-lithospheric LVZ in cratonic settings (Pontevivo and Thybo, 2006). SEMum has a pronounced mid-lithospheric LVZ, so the excellent fit between SEMum predictions and data strongly indicate that a mid-lithospheric LVZ is not incompatible with the available data. Furthermore, a number of phase velocity dispersion studies — which are methodologically and observationally independent from our work — indicate the presence of a mid-lithospheric low velocity in the sub-cratonic lithosphere: Slave Craton (Fig. 3 of Chen et al., 2007), the Baltic shield (Fig. 4b of Lebedev et al., 2009) and Tanzanian Craton (Fig. 8 of Weeraratne et al., 2003).

3.4. Oceanic structure

Three of the clusters are associated with oceanic crust. The slowest of these (OR1, red in Figs. 1e and 3c), is found beneath MORs and the back-arcs of subduction zones. It is also found beneath several specific continental settings: western North America, the Ethiopian segment of the East African Rift (EAR) and on both sides of the Red Sea. The OR1 velocity profile has a prominent LVZ reaching velocities as low as ~4.25 km at 100 km depth (Fig. 3d).

At the margins of the areas covered by this cluster, we find an interesting region (OR2, orange in Figs. 1e and 3c). This region comprises four northwest–southeast trending bands across the Pacific

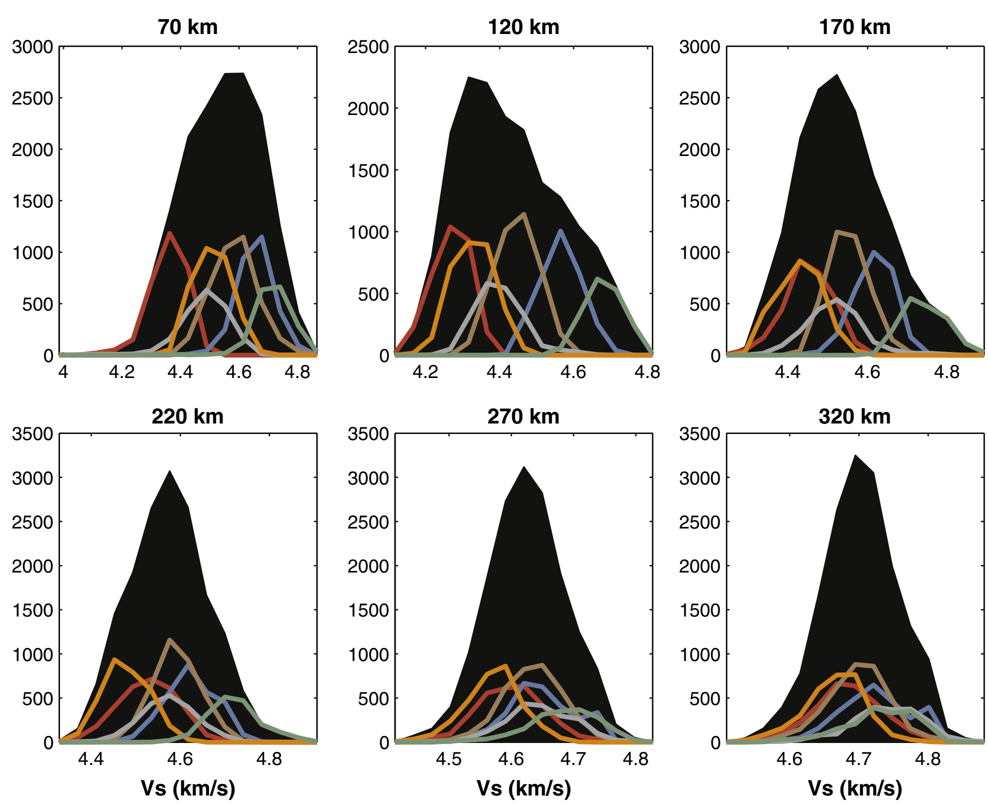

Fig. 8. Histograms of isotropic Vs present in SEMum (black) and in each of the clusters of the N = 6 regionalization (colored lines: OR1 red, OR2 orange, OR3 brown, CR1 green, CR2 blue, CR3 gray) at a set of 6 depths: 70 km, 120 km, 170 km, 220 km, 270 km, and 320 km. Note how the OR1 region changes from being slower than OR2 at depths <150 km, to being faster than OR2 at depths >170 km.

Table 1
Percent of ΔVs at 100 km depth retrieved by SEMum, SAW24B16 and S362ANI compared to values obtained in regional studies (A: (Gaherty, 2001); B: (Harmon et al., 2009); C: (Dugda et al., 2007)), which give a ΔVs of −0.3 km/s from a reference value taken as 4.4 km/s. A value of 100% would indicate full retrieval of velocity anomalies observed in regional studies. SEMum retrieves the amplitude of the low velocity anomalies more robustly than the other models.

Location	SEMum (%)	SAW24B16 (%)	S362ANI (%)
Reykjanes Ridge (A)	53	36	20
East Pacific Rise (B)	98	54	66
Afar Region (C)	57	38	37

basins, aligned with the direction of absolute plate motion in the hotspot reference frame (Argus and Gordon, 1991), including one in the vicinity of Hawai'i, and another near the Samoan and Tahiti hotspots (Fig. 7a). The alignment with absolute plate motion direction is not seen beneath the Atlantic or Indian oceans. Richter (1973) proposed that two scales of convection are present in the upper mantle, and that, after a sufficiently long time, the smaller scale convection would align along the plate motion direction. This is precisely the behavior revealed by cluster analysis in SEMum. Furthermore, the characteristic ~1000 km length-scale of the OR2 bands is consistent with gravity observations that have been interpreted as a signal of Richter Rolls beneath the Pacific (Marsch and Marsh, 1976). Furthermore, hotspots appear to be preferentially found in the vicinity of this region; 29 of the 38 hotspots are found within 5° distance from OR2.

In Fig. 8, we show histograms of isotropic Vs present in SEMum (black) and in each of the clusters of the N = 6 regionalization, colored according to the same scheme as Fig. 1e/3c. At 70 and 120 km depth, a comparison of velocity histograms for the OR1 (red) and OR2 (orange) regions reveals that OR2 has a weaker LVZ than OR1, with average velocities of ~4.35 km/s found at 125 km. However, below 150 km depth, OR2 becomes slower than OR1. If we define to the depth to the bottom of the oceanic LVZ (i.e. asthenosphere) by the steep positive gradient seen in all 3 oceanic regions, and centered around 170 km, this indicates that regions experiencing hotspot volcanism are closely associated with anomalously slow shear wave speeds in the sub-asthenospheric upper mantle. Indeed, even though differences between clusters decrease with depth, the OR2 region remains distinctly slower than the average, from 200 km to at least 300 km (Figs. 3d and 8). On the other hand, the CR1 region (i.e. the cratons) exhibits a less pronounced asthenospheric LVZ and remains faster than average until at least 300 km depth.

The final oceanic region (OR3) is associated with old oceanic crust (median age 91 Ma, brown in Fig. 1e). Its velocity profile falls near the middle between the cratonic profile of CR1 and the slow velocities associated with OR1. It is distinguished from CR3 in that its old, cold lithosphere is faster at shallow depths. OR3 has a weak LVZ, in which minimum velocities of ~4.43 km/s are observed between 100 and 125 km depth. In Fig. 8 (and also Fig. 3d) we can see that at most depths, the CR3 region (gray) is closest to the global average (black), except where it is biased toward slightly higher velocities by the signal of subducting slabs, which preferentially underlie tectonically active continents.

4. Discussion

We have applied cluster analysis to Vs and ξ profiles of a high-resolution, upper mantle tomographic model developed using the spectral element method. Regardless of whether a squared Euclidean or correlation distance measure is employed, *k-means* cluster analysis identifies several families of shear wave speed profiles that correspond to known tectonic provinces. The geographic extents of the families of similar Vs or ξ profiles extracted from different tomographic models can be readily compared and analyzed, allowing a straightforward means of exploring the salient features across tomographic models. By investigating differences between cluster geographic extents from tomography and those inferred from surface observations, anomalies and discrepancies can also be readily identified. Therefore, we propose that cluster analysis is a useful "meta-analysis" tool in the interpretation of seismic models.

The difference between our tomography-based mapping of shields and that based on surface observations may shed light on how the underlying cratonic roots and sub-continental lithosphere evolves. For example, the South African shield is mapped by SEMum to be further north than the associated South African shield in 3SMAC; this presents an interesting opportunity to investigate possible deformation of cratonic roots (Eaton and Frederiksen, 2007). Similarly, we find thick lithosphere beneath northern India and western Tibet, and not beneath southern India. This may be related to India's rapid northward motion and associated cratonic erosion (Kumar et al., 2007), and/or the underthrusting of the Indian lithosphere beneath Tibet (Friederich, 2003).

In addition to probing lithospheric structure, characteristic velocity profiles defined by the cluster analysis of SEMum can provide a reference for regional studies and for thermochemical interpretations of tomography based on mineral physics. This is because the mean of the velocity profiles that constitute an individual cluster is less likely to be affected by averaging of dissimilar structures that can result when regionalizations based on geologic and tectonic observations made at the surface are extrapolated to great depth. However, in order for these characteristic velocity profiles to serve as a reliable reference, the amplitude of velocity variations of the global model must be similar to those observed in regional and local studies. Because many global tomographic models did not retrieve the amplitude of lateral velocity variations inferred at smaller scales (Gudmundsson and Sambridge, 1998), we investigate whether this limitation of global models has been overcome in SEMum. Table 1 compares the amplitude of low-velocity anomalies obtained in SEMum, S362ANI, SAW24B16 at a depth of 100 km, against those observed in local studies (Dugda et al., 2007; Gaherty, 2001; Harmon et al., 2009). It confirms that at this depth, our SEM-based tomographic model is able to retrieve amplitudes of lateral variations in Vs that are in much closer agreement with values obtained in regional studies, than are the models developed with more approximate forward-modeling schemes. This demonstrates a key benefit of using very accurate forward modeling computations, in particular for low velocity regions, which are more susceptible to forward-modeling errors, and suggests that our ability to better retrieve accurate amplitudes of seismic anomalies will continue to improve as tomographers analyze larger datasets and adopt more sophisticated wave propagation schemes.

5. Conclusions

Cluster analysis of SEMum has demonstrated striking similarities in the depth profiles of major cratons, and confirmed the presence of a sub-continental mid-lithospheric low velocity zone in a global tomographic model. The cluster analysis also elucidated a close relationship between hotspots, anomalous ocean regions and the MORs, and found that the anomalous oceanic region (OR2) is characterized by reduced velocities (and presumably enhanced temperatures) at depths greater than 150 km. Interestingly, the only continental setting in which this anomalous oceanic region was found is beneath the Kenyan segment of the EAR. This indicates that ongoing continental rifting is likely associated with a deep mantle thermal source. Though the clusters we identify represent a novel starting point for understanding the variability and relationships between upper mantle structures, much more is to be learned from cluster analysis of higher resolution studies that can be achieved in the future by extending this and similar tomographic approaches to shorter periods.

Acknowledgments

The authors thank Huaiyu Yuan for helpful discussions and Adam Dziewonski for suggestions on improving this manuscript. Constructive comments by Peter Shearer, Goran Ekström, and an anonymous reviewer helped to focus and clarify the manuscript. Support for VL was provided by an NSF Graduate Research Fellowship. We acknowledge support from NSF through grant EAR-0738284. This is Berkeley Seismological Laboratory contribution 11-04.

References

Abt, D.L., Fischer, K.M., French, S.W., Ford, H.A., Yuan, H., Romanowicz, B., 2010. North American lithospheric discontinuity structure imaged by Ps and Sp receiver functions. J. Geophys. Res. 115. doi:10.1029/2009JB006914.
Argus, D., Gordon, R., 1991. No-net-rotation model of current plate velocities incorporating plate motion model NUVEL-1. Geophys. Res. Lett. 18 (11), 2039–2042.
Bozdağ, E., Trampert, J., 2008. On crustal corrections in surface wave tomography. Geophys. J. Int. 172 (3), 1066–1082.
Capdeville, Y., Chaljub, E., Vilotte, J.P., Montagner, J.P., 2003. Coupling the spectral element method with a modal solution for elastic wave propagation in global earth models. Geophys. J. Int. 152, 34–67.
Chen, C., Rondenay, S., Weeraratne, D.S., Snyder, D.B., 2007. New constraints on the upper mantle structure of the Slave craton from Rayleigh wave inversion. Geophys. Res. Lett. 34. doi:10.1029/2007GL029535.
Dugda, M.T., Nyblade, A.A., Julia, J., 2007. Thin lithosphere beneath the Ethiopian Plateau revealed by a joint inversion of Rayleigh wave group velocities and receiver functions. J. Geophys. Res. 112. doi:10.1029/2006JB004918.
Dumay, J., Fournier, F., 1988. Multivariate statistical analyses applied to seismic facies recognition. Geophysics 53 (9), 1151–1159.
Dziewonski, A.M., 1970. On regional difference in dispersion of mantle R ayleigh waves. Geophys. J. R. Astron. Soc. 22, 289–325.
Eaton, D.W., Frederiksen, A., 2007. Seismic evidence for convection-driven motion of the North American plate. Nature 446, 428–431.
Ekstrom, G., Tromp, J., Larson, E., 1997. Measurements and global models of surface wave observations. J. Geophys. Res. 102 (B4), 8137–8157.
Ford, H.A., Fischer, K.M., Abt, D.L., Rychert, C.A., Elkins-Tanton, L.T., 2010. The lithosphere–asthenosphere boundary and cratonic lithospheric layering beneath Australia from Sp wave imaging. Earth Planet. Sci. Lett. 300, 299–310.
Friederich, W., 2003. The S-velocity structure of the East Asian mantle from inversion of shear and surface waveforms. Geophys. J. Int. 153, 88–102.
Gaherty, J., 2001. Seismic evidence for hotspot-induced buoyant flow beneath the Reykjanes Ridge. Science 293, 1645–1647.
Gudmundsson, O., Sambridge, M., 1998. A regionalized upper mantle (RUM) seismic model. J. Geophys. Res. 103, 7121–7136.
Gung, Y., Panning, M., Romanowicz, B., 2003. Global anisotropy and the thickness of continents. Nature 422, 707–711.
Harmon, N., Forsyth, D.W., Weeraratne, D.S., 2009. Thickening of young Pacific lithosphere from high-resolution Rayleigh wave tomography: a test of the conductive cooling model. Earth Planet. Sci. Lett. 278, 96–106.
Houser, C., Masters, G., Shearer, P., Laske, G., 2008. Shear and compressional velocity models of the mantle from cluster analysis of long-period waveforms. Geophys. J. Int. 174, 195–212.
Jordan, T., 1981. Global tectonic regionalization for seismological data analysis. Bull. Seismol. Soc. Am. 71 (4), 1131.
Kanamori, H., 1970. Velocity and Q of mantle waves. Phys. Earth Planet. Int. 2, 259–275.
Karato, S., Jung, H., Katayama, I., Skemer, P., 2008. Geodynamic significance of seismic anisotropy of the upper mantle: new insights from laboratory studies. Annu. Rev. Earth Planet. Sci. 36, 59–95.
Komatitsch, D., Vilotte, J.P., 1998. The spectral element method: an efficient tool to simulate the seismic response of 2D and 3D geological structures. Bull. Seismol. Soc. Am. 88 (2), 368–392.
Komatitsch, D., Tromp, J., 2002. Spectral-element simulations of global seismic wave propagation: II. Three-dimensional models, oceans, rotation and self-gravitation. Geophys. J. Int. 150, 303–318.
Kumar, P., Yuan, X., Kumar, M.R., Rainer, K., Li, X., Chadha, R.K., 2007. The rapid drift of the Indian tectonic plate. Nature 449 (7164), 864–867.
Kustowski, B., Ekström, G., Dziewonski, A.M., 2008. Anisotropic shear-wave velocity structure of the earth's mantle: a global model. J. Geophys. Res. 113, B06306. doi:10.1029/2007JB005169.
Lebedev, S., Boonen, J., Trampert, J., 2009. Seismic structure of Precambrian lithosphere: new constraints from broad-band surface-wave dispersion. Lithos 109, 96–111.
Lekic, V., Panning, M., Romanowicz, B., 2010. A simple method for improving crustal corrections in waveform tomography. Geophys. J. Int. 182 (1), 265–278.
Lekic, V., Romanowicz, B., 2011. Inferring upper mantle structure by full waveform tomography with the Spectral Element Method. Geophys. J. Int. 185 (2), 799–831.
Li, X.-D., Romanowicz, B., 1995. Comparison of global waveform inversions with and without considering cross-branch modal coupling. Geophys. J. Int. 121, 695–709.
MacQueen, J., 1967. Some methods for classification and analysis of multivariate observations. Proc. Fifth Berkeley Symp. on Math. Statist. and Prob, 1, pp. 281–297.
Marsch, B.D., Marsh, J.G., 1976. On global gravity anomalies and two-scale mantle convection. J. Geophys. Res. 81 (29), 5267–5280.
Mégnin, C., Romanowicz, B., 2000. The three-dimensional shear velocity structure of the mantle from the inversion of body, surface and higher-mode waveforms. Geophys. J. Int. 143, 709–728.
Muller, R.D., 1997. Digital isochrons of the world's ocean floor. J. Geophys. Res. 102 (B2), 3211–3214.
Nataf, H., Ricard, Y., 1996. 3SMAC: an a priori tomographic model of the upper mantle based on geophysical modeling. Phys. Earth Planet. Inter. 95 (1), 101–122.
Okal, E., 1977. The effect of intrinsic oceanic upper-mantle heterogeneity on regionalization of long-period Rayleigh-wave phase velocities. Geophys. J. R. Astr. Soc. 49, 357–370.
Pontevivo, A., Thybo, H., 2006. Test of upper mantle low velocity layer in Siberia with surface waves. Tectonophysics 416, 113–131.
Plomerova, J., Kouba, D., Babuska, V., 2002. Mapping the lithosphere–asthenosphere boundary through changes in surface-wave anisotropy. Tectonophysics 358 (1), 175–185.
Richter, F.M., 1973. Convection and large-scale circulation of the mantle. J. Geophys. Res. 78 (35), 8735–8745.
Ritzwoller, M.H., Shapiro, N.M., Barmin, M.P., Levshin, A.L., 2002. Global surface wave diffraction tomography. J. Geophys. Res. 107 (B12). doi:10.1029/2002JB001777.
Romanowicz, B., 1991. Seismic tomography of the Earth's mantle. Annu. Rev. Earth Planet. Sci. 19 (1), 77–99.
Romanowicz, B., 2003. Global mantle tomography: progress status in the past 10 years. Annu. Rev. Earth Planet. Sci. 31, 303–328.
Romanowicz, B., 2009. The thickness of tectonic plates. Science 324 (5926), 474–476.
Romesburg, C.H., 1984. Cluster Analysis for Researchers. Lifetime Learning Publications, Belmont California0-534-03248-6.
Rychert, C., Shearer, P., 2009. A global view of the lithosphere asthenosphere boundary. Science 324 (5926), 495–498.
Spetzler, J., Trampert, J., Snieder, R., 2002. The effect of scattering in surface wave tomography. Geophys. J. Int. 149 (3), 755–767.
Steinberger, B., 2000. Plumes in a convecting mantle: models and observations for individual hotspots. J. Geophys. Res. 105 (B5), 11,127–11,152.
Thybo, H., Perchuc, E., 1997. The seismic 8° discontinuity and partial melting in the continental mantle. Science 275 (5306), 1626–1629.
Tronicke, J., Holinger, K., Barrash, W., Knoll, M.D., 2004. Multivariate analysis of cross-hole georadar velocity and attenuation tomograms for aquifer zonation. Water Resour. Res. 40 (W01519). doi:10.1029/2003WR002031.
Toksöz, M.N., Anderson, D.L., 1966. Phase velocities of long-period surface waves and structure of the upper mantle. I. Great-circle Love and Rayleigh wave data. J. Geophys. Res. 73, 3801–3806.
Weeraratne, D.S., Forsyth, D.W., Fischer, K.M., Nyblade, A.A., 2003. Evidence for an upper mantle plume beneath the Tanzanian craton from Rayleigh wave tomography. J. Geophys. Res. 108, 2427.
Yuan, H., Romanowicz, B., 2010. Lithospheric layering in the North American craton. Nature 466, 1063–1068.